PHYSICAL REVIEW B **93**, 140413(R) (2016)

Constructing a magnetic handle for antiferromagnetic manganites

Artur Glavic,[1,*] Hemant Dixit,[2,3] Valentino R. Cooper,[2] and Adam A. Aczel[4]

[1]*Laboratory for Neutron Scattering and Imaging, Paul Scherrer Institut, 5232 Villigen PSI, Switzerland*

[2]*Materials Science and Technology Division, Oak Ridge National Laboratory, P.O. Box 2008, MS6114, Oak Ridge, Tennessee 37831, USA*

[3]*GLOBALFOUNDRIES Engineering Private Limited, 9th Floor, N1 Building, Manyata Embassy Business Park, Bangalore, 560045 India*

[4]*Quantum Condensed Matter Division, Oak Ridge National Laboratory, P.O. Box 2008, MS6475, Oak Ridge, Tennessee 37831, USA*

(Received 13 December 2015; revised manuscript received 30 March 2016; published 27 April 2016)

An intrinsic property of antiferromagnetic materials is the compensation of the magnetic moments from the individual atoms that prohibits the direct interaction of the spin lattice with an external magnetic field. To overcome this limitation we have created artificial spin structures by heteroepitaxy between two bulk antiferromagnets $SrMnO_3$ and $NdMnO_3$. Here, we demonstrate that charge transfer at the interface results in the creation of thin ferromagnetic layers adjacent to *A*-type antiferromagnetism in thick $NdMnO_3$ layers. A novel interference based neutron diffraction technique and polarized neutron reflectometry are used to confirm the presence of ferromagnetism in the $SrMnO_3$ layers and to probe the relative alignment of antiferromagnetic spins induced by the coupling at the ferro- to antiferromagnet interface. A density functional theory analysis of the driving forces for the exchange reveals strong ferromagnetic interfacial coupling through quantifiable short range charge transfer. These results confirm a layer-by-layer control of magnetic arrangements that constitutes a promising step on a path towards isothermal magnetic control of antiferromagnetic arrangements as would be necessary in spin-based heterostructures like multiferroic devices.

DOI: 10.1103/PhysRevB.93.140413

Exchange coupling between ferromagnets (FM) and antiferromagnets (AFM) has been a field of intense study since the first observation of exchange bias (EB) in a FM/AFM composite system [1–3]. Many technical applications already rely on this effect [2,4] although a microscopic explanation of the physical origins is still under intense debate [2,3]. The intuitive image of direct exchange of FM spins to AFM spins at the interface, which would require uncompensated magnetic moments of the AFM, has been proven to fail by several observations of EB across fully compensated AFM interfaces [5,6]. This implies that EB is not the result of a direct coupling of AFM to FM spins, which is prohibitive for applications where a control of the AFM spin structure via magnetic fields is desired as, e.g., in multiferroic memory and sensing devices [7–10].

Here we try to overcome the limitations of EB through the artificial creation of FM/AFM heterostructures with strong exchange interactions between AFM and FM spins at the interface, introducing a "magnetic handle" to control the AFM isothermally. Such a goal can be achieved in transition metal oxide superlattices where FM is induced by electronic reconstruction, i.e., charge transfer at the interface. Perovskite oxides are still among the most studied and promising spin-based multiferroic materials in bulk [11–14] and thin films [15,16] recently even reaching ordering near and above room temperature [17,18]. Previous work on digital superlattices [integer number of monolayers (ML)] with a ratio 1:2 of the two AFM insulators $SrMnO_3$ (SMO) and $LaMnO_3$ (LMO), demonstrated that such interfacial electronic reconstruction leads to an artificial mixed valence compound which exhibits FM metallicity [19–25]. The intrinsic similarity between the double exchange paths of FM mixed valence manganites and their AFM parent compounds with superexchange produce the correct environment for the emergence of FM character. Here, the nearest neighbor exchange is established through the intermediary oxygen ions in an almost identical structural environment.

We explored the exchange coupling at the interface of the isoelectronic $NdMnO_3$ (NMO)/SMO superlattice with an increased NMO thickness of 11 MLs and 1–3 MLs of SMO. NMO has a lower bulk AFM ordering temperature than LMO, ensuring the FM spins are already ordered at the AFM transition. As NMO has an *A*-type AFM structure with alternating planes of parallel spins it is possible for all of its magnetic moments at the interface to align with the SMO spins. Using neutron reflectivity and diffraction we confirm the presence of FM in the SMO layers which are sandwiched by AFM arranged NMO layers. The studied systems are sketched in Fig. 1 to illustrate the magnetic order in the superlattice for an existing interlayer exchange. First principles calculations indicate that the charge transfer due to the mixed Mn valence induced by the Sr^{2+} and Nd^{3+} *A*-site cations is limited to only one or two MLs near the interface almost fully recovering the NMO bulk AFM structure by the center of the NMO block. Furthermore, this interfacial electronic reconstruction is correlated with the emergence of FM in the SMO layers. As such, the ability to control the movement and distribution of charge in the interfacial regions of such AFM superlattices may prove useful for designing the magnetic properties at the interface, thus opening the door to a number of applications.

Samples were grown on commercial $TbScO_3$ (0 0 1) substrates using pulsed laser deposition with in-situ RHEED control to define layer sequences. For details about sample preparation and characterization see Supplemental Material [26]. The samples used for the described experiment consisted of 40 repetitions of 11 ML NMO and 1, 2, and 3 ML SMO.

FM order at the SMO interface was measured using polarized neutron reflectometry, a technique to study magnetism of buried interfaces [27–32]. The measurements were done at Beamline 4A [33] of the SNS at ORNL, which operates

*artur.glavic@psi.ch

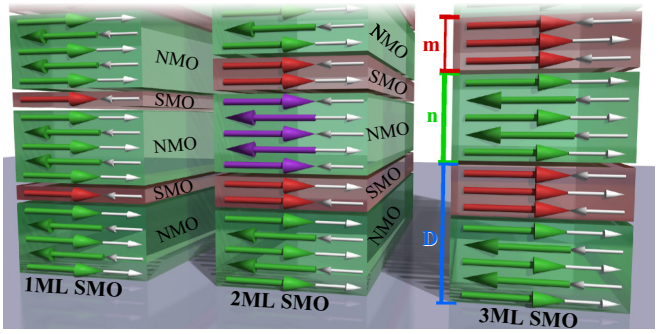

FIG. 1. Sketch of multilayer systems of $NdMnO_3$ and $SrMnO_3$ with different $SrMnO_3$ thicknesses. Gray arrows indicate the spin orientation in a purely A-type AFM system, green and purple the $NdMnO_3$ spins that align parallel and antiparallel with it. Every second AFM layer in the 2 ML sample has spins antiparallel to the continuous AFM structure, leading to destructive interference in neutron diffraction.

in the time of flight mode and utilizes a reflecting supermirror polarizer and radio frequency spin flipper to define and manipulate the incident neutron polarization. The reflectivities for spin-up and spin-down polarized neutron beams are shown in Fig. 2. X-ray and neutron reflectometry data were refined with the same structural model using the GenX program [34] including small thickness variations between sample center and edges. The oscillations at small Q_z correspond to the total film thickness, while the position of the Bragg peaks around 0.15 $Å^{-1}$ is given by the bilayer periodicity. Nd and Sr have similar nuclear scattering lengths resulting in negligible contrast for neutron reflectometry and no visible Bragg-peak in the nonmagnetic state. The presence of a Bragg-peak in all three measurements is therefore an indication of magnetic contrast between NMO and SMO from a variation of magnetization between the two constituents. A variation in saturation magnetization throughout the heterostructure leads to the asymmetry between spin-up and spin-down Bragg peaks. The splitting

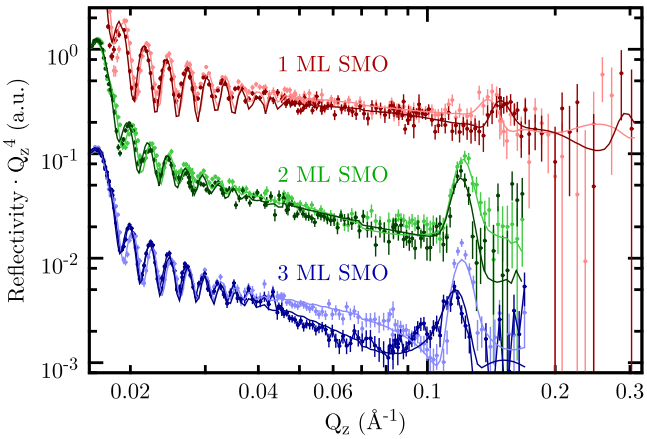

FIG. 2. $[11\,\text{ML-NdMnO}_3/1|2|3\,\text{ML-SrMnO}_3]_{x40}$ superlattices on $TbScO_3$ measured with polarized neutron reflectometry at 20 K with a 100 mT field. Spin-up neutron polarization is shown in brighter colors than the corresponding spin-down measurements. Solid lines are fits to the data.

of spin-up and spin-down reflectivity close to the plateau of total reflection further indicates the presence of a macroscopic magnetic moment throughout the superlattice. The fits are consistent with the SMO layers and one additional ML of NMO being magnetic, with no measurable ferromagnetism within the remaining NMO blocks. Although it is not possible to precisely define the magnetic moment of the layers due to the influence of roughness and the variation of the moment through the superlattice it is on the order of $1\mu_B$/Mn and thus much larger than the magnetization within a canted AFM.

While the direct observation of the alignment of the AFM structure to the FM layers is not possible, the coupling across the interface will result in a coherent alignment of the AFM layers within the superlattice. In samples with sufficient superlattice repetitions, neutron diffraction can then be used to observe the long range AFM correlations. The magnetic structure factor S_M for a given number of monolayers can be calculated analytically, which has been carried out in the supplemental information. For coherent magnetic ordering the (0 0 1)-peak of the superlattice only has significant intensity for an odd number of SMO layers. A qualitative understanding of the destructive interference for even m-SMO layers is evident from Fig. 1 as every second NMO block has spins antiparallel to a purely AFM structure in contrast to odd m systems where all NMO blocks are aligned parallel to it.

The fact that the AFM structure factor only depends on the SMO thickness allows us to test whether FM coupling occurs using neutron diffraction from a set of three samples with 1, 2, and 3 ML of SMO. In the presence of interlayer exchange coupling we would expect to observe a sharp AFM Bragg peak at the (0 0 1) position for 1 and 3 ML SMO and no magnetic scattering for 2 ML SMO. A system without such a coupling would have random relative orientations of AFM domains for each block and would thus result in broad AFM peaks (width $\approx \frac{2\pi}{n} = 0.15$ $Å^{-1}$) with low intensities that were independent of the SMO layer thickness.

For these experiments the triple-axis spectrometer HB1A at HFIR of ORNL was used. Figure 3 depicts neutron diffraction measured on the 1 ML SMO sample at 20 K and 8 K. After subtraction of the structural (0 0 1) reflection [35], an AFM peak is visible in each measurement. The correlation length of the magnetic structure is inversely related to the natural Lorentzian peak width ($\xi = \frac{2\pi}{\gamma}$). As the substrate structural peak can be well described with two Gaussians (instrument resolution and crystal twinning) two Voigt functions were used to fit the magnetic peaks, using the same Gaussian width, relative peak intensity and Q separation and constraining γ to be equal. The resulting fits, shown in Fig. 3, yield γ values of $8(3)\times10^{-3}$ $Å^{-1}$ (20 K) and $13(2)\times10^{-3}$ $Å^{-1}$ (8 K) corresponding to correlation lengths of 79 nm and 48 nm (19 and 12 bilayers), respectively. Scattering from randomly oriented AFM domains of uncoupled NMO layers would have a correlation length of 1–2 bilayers, thus proving a coherent AFM structure throughout the superlattice.

Temperature dependent measurements at the Q position indicated as $I(T)$ in Fig. 3 were measured for all three samples to extract the temperature dependent magnetic order parameter (see Fig. 4). Due to the large magnetic moment of Tb the substrates produced a strong temperature dependent paramagnetic

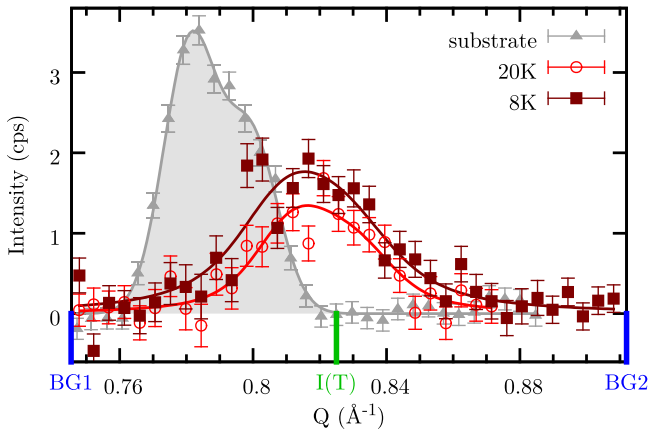

FIG. 3. Neutron diffraction Θ-2Θ scan around AFM (0 0 1) peak from [11 ML-$NdMnO_3$/1 ML-$SrMnO_3$]$_{x40}$. The gray data and shaded area indicate the 100 K measurement of the structural substrate reflection that was subtracted from the lower T data presented here. Solid lines through the low T data indicate fits to two Voigt functions using the same Gaussian widths, relative peak intensity, and peak separation obtained from first fitting the substrate reflection.

background, therefore the temperature dependent intensity was measured on the Bragg peak and at 0.08 Å^{-1} larger and smaller Q values (indicated in Fig. 3 on the x axis as I(T) and BG1/2). The background measurement was then fit with an empirical $\frac{a}{T-b} + c \cdot T + d$ function and subtracted from the peak intensity to retrieve the results of Figs. 3 and 4. There is a transition at ≈80K for the 1 ML and 3 ML SMO samples and no magnetic signal for the 2 ML system, a clear indication of the coherent alignment of neighboring AFM layer spins to each other as was expected for a multilayer with exchange-coupled FM and AFM layers.

In order to understand the magnetic couplings at the NMO/SMO interface, we performed first-principles calculations using density functional theory (DFT) within the generalized gradient approximation (GGA) and the projector augmented plane-wave (PAW) method [36,37] as implemented in the VASP package [38,39]. An energy cutoff of 520 eV was used with a Monkhorst-Pack special k-point grid of $6 \times 6 \times 4$ for bulk and $6 \times 6 \times 1$ for superlattices. Ions were relaxed until the forces on each atomic site were below 10 meV/ Å and simultaneously achieving a total energy convergence of 10^{-6} eV. We used a $\sqrt{2} \times \sqrt{2} \times 2$ unit cell to describe the bulk orthorhombic cell ($Pbnm$ space group). The total energies of the superlattices with ferromagnetic and antiferromagnetic couplings across the interface are mapped onto a classical Heisenberg Hamiltonian for the nearest-neighbor magnetic exchange interactions within the orthorhombic a-b plane (J_{ab}) and along the c direction (J_c):

$$H = -\frac{1}{2}\sum_{i \neq j} J_{ij} S_i \cdot S_j$$

Here, $S = 2$ and the in-plane and out-of-plane exchange can be computed using

$$E_{A-AFM} - E_{FM} = S \times (\text{no. of bonds}) \times (\text{no. of sites}) \cdot J_c$$

$$E_{C-AFM} - E_{FM} = S \times (\text{no. of bonds}) \times (\text{no. of sites}) \cdot J_{ab}$$

First, we studied bulk NMO to find a valid approach for the later superlattice investigations. The inability of the generalized gradient approximation (GGA) or GGA+U approach to predict the correct magnetic order in $R$$MnO_3$ manganites (R=La, Pr, Nd, Sm, Eu, Gd) has been pointed out in the literature [40–42]. Indeed, using GGA in DFT we obtain a ferromagnetic ground state for bulk NMO at the theoretically optimized structure instead of an A-type antiferromagnetic solution. The overestimation of lattice parameters and bond angles results in reduced out-of-plane exchange, stabilizing the ferromagnetic order. At the experimental lattice geometry with fully relaxed atomic positions, however, we retain the correct A-type antiferromagnetic order for bulk NMO with GGA. Furthermore, the calculated Heisenberg exchange parameters in terms of the nearest-neighbor magnetic exchange interactions for bulk NMO are $J_c = -0.47$ meV and $J_{ab} = 3.21$ meV, which compare well with those calculated using a hybrid functional (HSE06) ($J_c = -0.28$ meV and $J_{ab} = 2.00$ meV [40]). But, as a consequence of the overestimated exchange parameters, we obtain a Néel temperature of 127 K compared to the experimental value of 85 K using a mean-field description. Since the A-type AFM solution can only be obtained with the experimental lattice parameters, these experimental lattice constants are used to study the magnetic coupling in SMO/NMO superlattices. We considered three superlattices with composition m-SMO/7-NMO where $m = 1,2,3$ [Figure 5(a)] to model the superlattices grown on $TbScO_3$, where the layers at the interface were intermixed with 50% of Sr and 50% of Nd in a checkerboard pattern. This geometry was chosen as the exact atomic structure of the films at the interface is unknown. However, it is symmetric around the layer centers and allows for a clear assignment of Mn moments to specific MLs. Similar results were obtained by modeling systems with sharp SMO/NMO interfaces.

In addition to the bulk NMO and SMO systems, that were simulated for comparison, three types of magnetic orderings: (1) a completely ferromagnetic superlattice, (2) a mixed system with A-type AFM arrangement in the NMO layer, FM within SMO and FM across the SMO/NMO interface, and (3) a mixed system with the same interlayer arrangements as in case (2) but AFM across the SMO/NMO interface

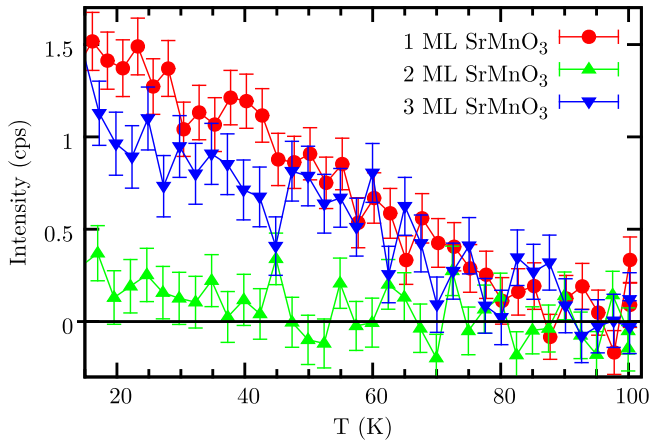

FIG. 4. Temperature dependent intensity at (0 0 1) from [11 ML-$NdMnO_3$/1|2|3 ML-$SrMnO_3$]$_{x40}$ measured with neutron diffraction.

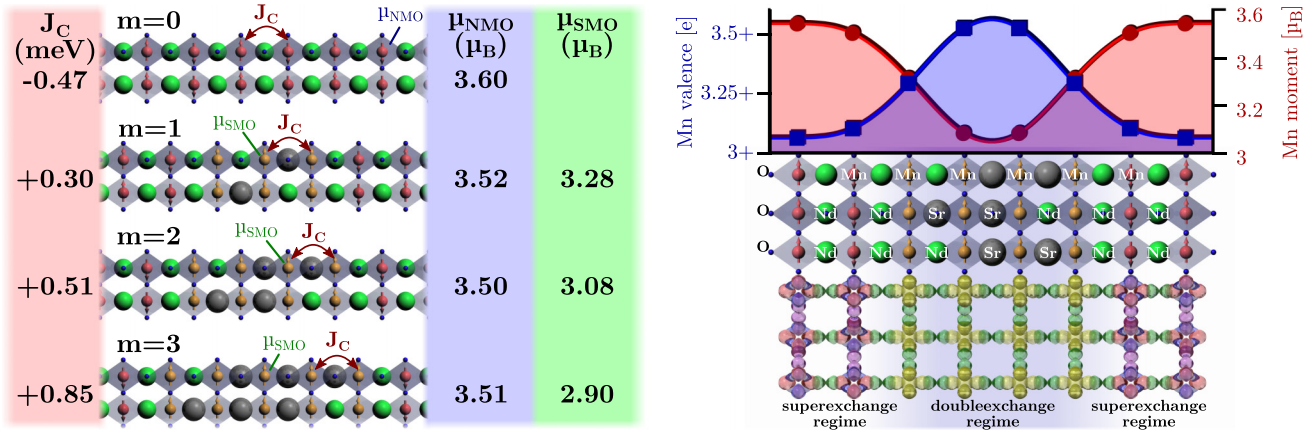

FIG. 5. Results of density functional theory calculations for NMO_7/SMO_m superlattices using GGA. The c-lattice direction is shown horizontally. (a) Sketch of the interface region of the 4 simulations with effective exchange along the c-axis (J_C) and the magnetic moments on the Mn-ions furthest away from the interface μ_{SMO}/μ_{NMO}. (b) Mn charge occupancy (blue squares) and magnetic moment (red circles) for the $m = 2$ simulation (top) with a sketch of the interface atoms and orbitals (bottom).

were investigated. Our systematic GGA calculations for the SMO/NMO superlattices indicate that FM coupling across the SMO/NMO interface has lower energy compared to an AFM coupling for the 1, 2, and 3 SMO cases. Of course, the SMO layers may remain antiferromagnetic in the bilayer and trilayer cases. However, in both cases the antiferromagnetic solution within the SMO block did not converge, and therefore for the purpose of understanding the experimental results we only considered FM SMO layers in these systems. Nevertheless, although both bulk NMO and SMO are A- and G-type antiferromagnets, respectively, their superlattices reveal a ferromagnetic coupling across the interface.

The calculated strength of the interlayer out-of-plane exchange (J_C) is shown in Fig. 5(a), summarized together with the magnetic moments for antiferromagnetically ordered NMO and ferromagnetically ordered SMO layers. Here, we find that the ferromagnetic exchange coupling between SMO and NMO increases and the SMO magnetic moment decreases with the number of SMO layers, while the NMO magnetic moment remains nearly constant. This is a consequence of charge accumulation in the interfacial region due to the charge difference between Sr^{2+} and Nd^{3+} cations, similar to that observed in the La δ-doped $SrTiO_3$ 2DEG systems [43,44].

Due to the strong p-d hybridization between the O-p and Mn-d states, the charge transfer within the NMO/SMO superlattice cannot be precisely determined using formal approaches such as Bader charge analysis. Hence, we rely on an alternative method to calculate the valence shown in Fig. 5(b) in which the difference between the integrated magnetic moments on Mn atoms in each layer and the Mn magnetic moment in bulk NMO is added with the formal valence charge of 3+ of the Mn atom to estimate the charge transfer in each layer in the superlattice. Such a method is known to be sufficiently accurate to calculate the layer-by-layer charge transfer in oxide heterostructures and superlattices [45]. A closer look into the electronic reconstruction [Fig. 5(b)], shows that the Mn valence and magnetic moment variation across the interface for the two ML SMO system extends to roughly three unit cells away from the center of the SMO layer. The Mn charge state and magnetic moment recovers quickly within the NMO layer, allowing the presence of orbital and AFM order already in the second Mn layer within the NMO structure. The third Mn layer only has 0.1 e higher oxidation than the bulk NMO. This is very similar to the charge distribution observed in the oxide 2DEG systems [46–48] or the superlattices studied by Nanda and Satpathy [49], where the magnetic moments near the interface are similar and the coupling follows the same trend. In both systems, the charge transfer at the interface induces magnetic moments on the interfacial Mn atoms in the SMO layer.

In summary, we have shown that it is possible to create an artificial AFM/FM heterostructure with a direct exchange coupling of FM to AFM spins at the interface. Such a structure could be used to directly influence the spin arrangement within an AFM layer by applying an external magnetic field without a change of temperature, as it is considerably different from the coupling achieved in exchange bias materials. An example would be a multiferroic spiral (e.g., $TbMnO_3$), where the spin direction at the interface is rotated to change the spiral chirality and with it the direction of the ferroelectric polarization.

Making use of interference neutron diffraction in conjunction with layer controlled growth of specifically designed structures, it is now possible to measure the relative alignment of AFM layers in a broad class of heterostructures. In conjunction with first principle calculations, this allows a deeper insight into complex magnetism in thin superlattices. The presence of a FM system that acts on AFM spins like a "handle" allows the manipulation of the AFM structures, thus adding an AFM reference layer to the superlattices, it might even be possible to observe switching of AFM spins with external magnetic fields in similar heterostructures.

Furthermore, we find that the electronic reconstruction at the interface (i.e., the movement of charge) is strongly coupled to the interfacial spin state and therefore can be used for tuning the magnetic properties at the interface. These findings are of importance to fundamental research

of magnetic interface effects in complex heterostructures as well as to investigations for the development of applications, where charge-spin coupling can be exploited or the control of AFM spins with magnetic field is desired, like magnetoelectric multiferroic devices.

We want to thank Satoshi Okamoto for useful discussion related to the analysis of the theoretical results and the late Michael Biegalski for his support during the PLD growth. A portion of this research at ORNL's High Flux Isotope Reactor and Spallation Neutron Source was sponsored by the Scientific User Facilities Division, Office of Basic Energy Sciences, US Department of Energy. Sample preparation and characterization for this research was conducted at the Center for Nanophase Materials Sciences, which is a DOE Office of Science User Facility. H.D. and V.R.C were supported by the U.S. Department of Energy, Office of Science, Basic Energy Sciences, Materials Sciences and Engineering Division through the Office of Science Early Career Research Program (V.R.C). This research used resources of the National Energy Research Scientific Computing Center, a DOE Office of Science User Facility supported by the Office of Science of the U.S. Department of Energy under Contract No. DE-AC02-05CH11231.

[1] W. H. Meiklejohn and C. P. Bean, Phys. Rev. **105**, 904 (1957).
[2] J. Nogués and I. K. Schuller, J. Magn. Magn. Mater. **192**, 203 (1999).
[3] M. Kiwi, J. Magn. Magn. Mater. **234**, 584 (2001).
[4] J. C. S. Kools, IEEE Trans. Magn. **32**, 3165 (1996).
[5] A. E. Berkowitz and J. H. Greiner, J. Appl. Phys. **36**, 3330 (1965).
[6] T. J. Moran, J. M. Gallego, and I. K. Schuller, J. Appl. Phys. **78**, 1887 (1995).
[7] R. Ramesh and N. A. Spaldin, Nat. Mater. **6**, 21 (2007).
[8] P. Jain, Q. Wang, M. Roldan, A. Glavic, V. Lauter, C. Urban, Z. Bi, T. Ahmed, J. Zhu, M. Varela, Q. X. Jia, and M. R. Fitzsimmons, Sci. Rep. **5**, 9089 (2015).
[9] M. Bibes and A. Barthelemy, Nat. Mater. **7**, 425 (2008).
[10] T. Kimura, T. Goto, H. Shintani, K. Ishizaka, T. Arima, and Y. Tokura, Nature (London) **426**, 55 (2003).
[11] T. Aoyama, K. Yamauchi, A. Iyama, S. Picozzi, K. Shimizu, and T. Kimura, Nat. Commun. **5**, 4927 (2014).
[12] H. Das, A. L. Wysocki, Y. Geng, W. Wu, and C. J. Fennie, Nat. Commun. **5**, 2998 (2014).
[13] N. S. Fedorova, C. Ederer, N. A. Spaldin, and A. Scaramucci, Phys. Rev. B **91**, 165122 (2015).
[14] J. Young, A. Stroppa, S. Picozzi, and J. M. Rondinelli, J. Phys.: Condens. Matter **27**, 283202 (2015).
[15] E. Bousquet, M. Dawber, N. Stucki, C. Lichtensteiger, P. Hermet, S. Gariglio, J.-M. Triscone, and P. Ghosez, Nature (London) **452**, 732 (2008).
[16] J. Fontcuberta, Comptes Rendus Physique **16**, 204 (2015).
[17] M. J. Pitcher, P. Mandal, M. S. Dyer, J. Alaria, P. Borisov, H. Niu, J. B. Claridge, and M. J. Rosseinsky, Science **347**, 420 (2015).
[18] H. J. Zhao, W. Ren, Y. Yang, J. Íñiguez, X. M. Chen, and L. Bellaiche, Nat. Commun. **5**, 4021 (2014).
[19] P. Salvador, A. Haghiri-Gosnet, B. Mercey, M. Hervieu, and B. Raveau, Appl. Phys. Lett. **75**, 2638 (1999).
[20] A. Bhattacharya, X. Zhai, M. Warusawithana, J. N. Eckstein, and S. D. Bader, Appl. Phys. Lett. **90**, 222503 (2007).
[21] S. Dong, R. Yu, S. Yunoki, G. Alvarez, J. M. Liu, and E. Dagotto, Phys. Rev. B **78**, 201102 (2008).
[22] E. J. Monkman, C. Adamo, J. A. Mundy, D. E. Shai, J. W. Harter, D. W. Shen, B. Burganov, D. A. Muller, D. G. Schlom, and K. M. Shen, Nat. Mater. **11**, 855 (2012).
[23] A. Perucchi, L. Baldassarre, A. Nucara, P. Calvani, C. Adamo, D. G. Schlom, P. Orgiani, L. Maritato, and S. Lupi, Nano Lett. **10**, 4819 (2010).
[24] S. Smadici, B. B. Nelson-Cheeseman, A. Bhattacharya, and P. Abbamonte, Phys. Rev. B **86**, 174427 (2012).
[25] K. Pradhan and A. P. Kampf, Phys. Rev. B **87**, 155152 (2013).
[26] See Supplemental Material at http://link.aps.org/supplemental/10.1103/PhysRevB.93.140413 for additional information on sample preparation and structural characterization.
[27] T. J. Hicks, Adv. Phys. **45**, 243 (1996).
[28] O. Halpern and M. H. Johnson, Phys. Rev. **55**, 898 (1939).
[29] S. W. Lovesey, *Theory of Neutron Scattering from Condensed Matter: Volume 2: Polarization Effects and Magnetic Scattering*. The International Series of Monographs on Physics (Oxford University Press, New York, 1986).
[30] S. Maleev, V. Bar'yakhtar, and R. Suris, Sov. Phys. Solid State **4**, 2533 (1963).
[31] U. Rücker, E. Kentzinger, B. Toperverg, F. Ott, and T. Brückel, Appl. Phys. A **74**, S607 (2002).
[32] B. P. Toperverg, Physica B **297**, 160 (2001).
[33] H. Ambaye, R. Goyette, A. Parizzi, and F. Klose, Neutron News **19**, 11 (2008).
[34] M. Bjorck and G. Andersson, J. Appl. Crystallogr. **40**, 1174 (2007).
[35] Although the (0 0 1) Bragg peak is generally forbidden in the *Pbnm* space group of $TbScO_3$ crystal imperfections in the substrate result in finite intensity. A second contribution at this position is the small $\lambda/2$ contamination in the incident neutron beam.
[36] G. Kresse and D. Joubert, Phys. Rev. B **59**, 1758 (1999).
[37] P. E. Blöchl, Phys. Rev. B **50**, 17953 (1994).
[38] G. Kresse and J. Furthmüller, Phys. Rev. B **54**, 11169 (1996).
[39] G. Kresse and J. Furthmüller, Comput. Mater. Sci. **6**, 15 (1996).
[40] M. S. Sathyanarayana, Ph.D. thesis, University of Vienna, Austria, 2013.
[41] Q. Zhang, S. Dong, B. Wang, and S. Yunoki, Phys. Rev. B **86**, 094403 (2012).
[42] K. Yamauchi, F. Freimuth, S. Blügel, and S. Picozzi, Phys. Rev. B **78**, 014403 (2008).
[43] V. R. Cooper, Phys. Rev. B **85**, 235109 (2012).

[44] J. S. Kim, S. S. A. Seo, M. F. Chisholm, R. K. Kremer, H.-U. Habermeier, B. Keimer, and H. N. Lee, Phys. Rev. B **82**, 201407 (2010).

[45] S. Okamoto, A. J. Millis, and N. A. Spaldin, Phys. Rev. Lett. **97**, 056802 (2006).

[46] A. F. Santander-Syro, O. Copie, T. Kondo, F. Fortuna, S. Pailhes, R. Weht, X. G. Qiu, F. Bertran, A. Nicolaou *et al.*, Nature (London) **469**, 189 (2011).

[47] C. Cantoni, J. Gazquez, F. Miletto Granozio, M. P. Oxley, M. Varela, A. R. Lupini, S. J. Pennycook, C. Aruta, U. S. di Uccio *et al.*, Adv. Mater. **24**, 3952 (2012).

[48] H. W. Jang, D. A. Felker, C. W. Bark, Y. Wang, M. K. Niranjan, C. T. Nelson, Y. Zhang, D. Su, C. M. Folkman *et al.*, Science **331**, 886 (2011).

[49] B. R. K. Nanda and S. Satpathy, Phys. Rev. B **79**, 054428 (2009).